Efficient Rotation Invariant Feature Extraction for Texture Segmentation - via Multiscale Wavelet Frames

Mausumi Acharyya*and Malay K. Kundu
Machine Intelligence Unit, Indian Statistical Institute
203, B. T. Road, Calcutta - 700 035, INDIA
{res9522, malay}@isical.ac.in

Abstract

This work presents an approach to the extraction of rotation invariant features for texture segmentation using multiscale wavelet frame analysis. The texture is decomposed into a set of bandpass channels by a circularly symmetric wavelet filter, which then gives a measure of edge magnitudes of the texture at different scales. The texture is characterized by local energies over small overlapping windows around each pixel at different scales. This gives features that are rotation invariant and describe the scale-space signature of the texture. A simple clustering algorithm is applied to this signature to achieve the desired segmentation.

Index- Feature extraction, texture segmentation, wavelet transform, wavelet frames, non-separable filters.

1 Introduction

Texture analysis plays an important role in computer vision and pattern recognition and is widely applied to many areas like remote sensing, biomedical image processing, query by content in large image databases etc. A wide variety of texture analysis methods have been proposed in the past [1]. Earlier approaches focused on the analysis of the first-order or second-order statistics of textures, Gauss-Markov random field, local linear transforms.

Recently multiresolution and multiscale methods have been extensively studied [2] [3]. Multiresolution techniques intend to transform images into representation in which both frequency and spatial information is present. Wavelet transform provides a unifying framework for the analysis and characterization of images at different scales [4]. These recent findings have motivated several important studies for texture analysis [5] [6].

The majority of the existing work on texture analysis assumes that all images are acquired from the same view point. Practically this is an unrealistic assumption. A texture analysis approach should ideally be invariant to orientation of the texture. Extraction of rotation invariant texture features is a very difficult task. Kashyap *et.al* [7] first recognized the importance of rotation-invariant texture feature extraction. He developed a texture classification scheme based on autoregressive (AR) model. But the difficulty with their model is that, it could not be used for textures with strong anisotropy. To overcome this problem they incorporated two AR models, but still this did not suffice, because features derived from this type of AR models are invariant to rotations which are multiples of 45^0.

Cohen *et.al.* [8] modeled textures as Gaussian Markov random fields and used the maximum likelihood (ML) method to estimate coefficients and rotation angles. The problem with this method is that the likelihood function is highly nonlinear and local minima may exist, also this algorithm is computationally very intensive.

Chen and Kundu [3] used multichannel subband decomposition and a hidden Markov model (HMM) to solve this problem. The two dimensional (2-D) images were decomposed into subbands using quadrature mirror filter (QMF) bank, and modeled features of these subband images as an HMM. Texture samples with different orientations are treated to be in the same class. But it is obvious that for an image the signal components in each subband will be different for different orientations. So variability in texture feature vectors increases with increase in the number of textures to be analyzed.

Wu *et.al* [9] tried to solve this problem by converting the 2-D textured images into one dimensional (1-D) signals by spiral resampling, then QMF banks is used to decompose the signal. High order autocorrelation functions are taken as features and these features are modeled as an HMM. That is in this

*corresponding author

case rotational-invariance is simulated as translation-invariance. But this method too is computationally expensive.

Another approach to rotation-invariant texture feature extraction could be the implementation of non-separable filter banks using non-separable subsampling lattices in the decomposition scheme like the quincunx lattice, but still it is very difficult to get sufficient angular localization in this way.

Most recently Fountain *et.al* [10] have worked on rotation invariant texture features by taking the Fourier transform (FT) of the gradient direction histograms of the textures. The direction histograms being a periodic function of 2π, a rotation of the image is reflected as a translation of this histogram function. Therefore magnitudes of the FT of this function provides rotation invariant features.

But inspite of all these efforts we are of the opinion that if features are extracted from the texture itself and if by some means it is possible that the features themselves contain the rotational information, then we can get much improved results. This appears to be a more general method to cope with this problem and is precisely what we try to achieve in this paper.

In the present work, texture properties are characterized by wavelet frame analysis mainly as suggested in [11]. While discrete wavelet transform gives a non redundant representation of the textures, the discrete wavelet frame uses an overcomplete representation. This technique is employed to study the performance of a texture segmentation problem with respect to rotational invariance.

A fast and powerful scheme for implementing the 1-D - discrete wavelet transform (DWT) using a filter-bank has been designed [4] [12]. The 2-D extension is obtained in two steps by successive application of the 1-D filtering along rows and columns of an image. Due to the separable nature of implementation of the two dimensional discrete wavelet transform, it is strongly oriented in the horizontal and vertical directions. Such a decomposition cannot efficiently characterize directions other than 0^0 and 90^0. This is particularly inadequate while dealing with oriented textures. So what we need is a non-separable nature of implementation of the wavelet transform in 2-D. We make use of a wavelet filter which is circularly symmetric and hence is invariant to rotation.

In the next section, we review the wavelet frame decomposition. Section 3 describes the wavelet parameter computation which gives the features for texture discrimination and integration of these features. In section 4 we present our results and critical remarks about the performance and finally conclude our study.

2 Wavelet transforms and frames

2.1 Discrete wavelet transform

The wavelet decomposition can be interpreted as signal decomposition in a set of independent, spatially oriented frequency channels. Under these constraints an efficient real space implementation of the transform using quadrature mirror filter exists [4]. The discrete normalized scaling and wavelet basis functions are defined as,

$$\begin{array}{rcl} \phi_{i,k}(l) & = & 2^{i/2} h_i(2^i l - k) \\ \psi_{i,k}(l) & = & 2^{i/2} g_i(2^i l - k) \end{array} \quad (1)$$

where i and k are the dilation and translation parameters and h_i and g_i are respectively the sequence of lowpass and bandpass filters of increasing width indexed by i, which are expanded by inserting an appropriate number of zeros between taps and satisfy the quadrature mirror filter condition. The full discrete wavelet expansion of a signal $x \in l_2$ (l_2 is the space of square summable functions) is given as,

$$x(l) = \sum_{k \in Z} c_{(d_0)}(k)\phi_{d_0,k} + \sum_{i=1}^{d_0} \sum_{k \in Z} d_{(i)}(k)\psi_{i,k} \quad (2)$$

$d_{(i)}$'s are the wavelet coefficients and $c_{(d_0)}$'s are the expansion coefficients of the coarser signal approximation $x_{(d_0)}$. The c_{d_0}'s and d_i's can be interpreted in terms of simple filtering and downsampling operations.

$$\left\{ \begin{array}{rcl} c_{(d_0)}(k) & = & 2^{d_0/2}[h_{d_0}^T * x]_{\downarrow 2^{d_0}(k)} \\ d_{(i)}(k) & = & 2^{i/2}[g_i^T * x]_{\downarrow 2^i(k)} \text{ for } i = 1, \cdots, d_0 \end{array} \right. \quad (3)$$

where the symbol ^{T} denotes the transpose operation ($i.e. h^T(k) = h(-k)$) and where $[.] \downarrow m$ is the downsampling by factor m. In practice the 2-D DWT is computed by applying a separable filter bank to the image.

$$c_i(x,y) = [h_{i,x} * [h_{i,y} * c_{i-1}]_{\downarrow 2,1}]_{\downarrow 1,2}(x,y) \quad (4)$$
$$d_i^1(x,y) = [h_{i,x} * [g_{i,y} * c_{i-1}]_{\downarrow 2,1}]_{\downarrow 1,2}(x,y) \quad (5)$$
$$d_i^2(x,y) = [g_{i,x} * [h_{i,y} * c_{i-1}]_{\downarrow 2,1}]_{\downarrow 1,2}(x,y) \quad (6)$$
$$d_i^3(x,y) = [g_{i,x} * [g_{i,y} * c_{i-1}]_{\downarrow 2,1}]_{\downarrow 1,2}(x,y) \quad (7)$$

$*$ denotes the convolution operator, $\downarrow 2,1$ ($\downarrow 1,2$) denote subsampling along the rows (columns) and $c_0 = I(x,y)$ the original 2-D signal. $h_{i,x}$ ($g_{i,x}$) and $h_{i,y}$ ($g_{i,y}$) are the lowpass (bandpass) filtering along x and y directions respectively corresponding to different scale. $c_i(x,y)$ corresponds to the lowest frequencies, the d_i^n are obtained by bandpass filtering

in a specific direction and thus contain the detail information at scale i. $d_i^1(x,y)$ corresponds to the vertical high frequencies (horizontal edges), $d_i^2(x,y)$ the horizontal high frequencies (vertical edges) and $d_i^3(x,y)$ the high frequencies in both direction (the corners). $I(x,y)$ is represented at several scales by, $\{c_{d_0}, d_i^n \mid n = 1,2,3, i = 1,\ldots,d_0\}$

2.2 Wavelet Frames

Wavelet frame leads to an overcomplete decomposition of the signal

$$\begin{cases} d_i^{DWF}(k) &= \langle g_i(l-k).x(l)\rangle_{l_2} \\ c_{d_0}^{DWF}(k) &= \langle h_d(l-k).x(l)\rangle_{l_2} \end{cases} \quad (8)$$

Due to the special structure of the analysis filter bank, this decomposition has an interesting property of energy conservation. The frame is a spanning set, that requires finite limits on an inequality bound of inner products. If we want the coefficient in an expansion of a signal to represent the signal well, these coefficients should have certain properties, that are stated best in terms of energy and energy bounds.

The family of sequences $F = \{g_1(l-k), \cdots, g_{d_0}(l-k), h_{d_0}(l-k)\}$ constitutes a frame of the Hilbert space l_2, if there exists two constants $A > 0$ and $B < \infty$ such that,

$$\begin{aligned} &A \;.\; \|x\|_{l_2}^2 \;\leq\; \textstyle\sum_{k\,\in\,Z} \langle x(l), h_d(l-k)\rangle^2 \\ &+ \textstyle\sum_{i=1}^{d_0} \sum_{k\,\in\,Z} \langle x(l), g_i(l-k)\rangle^2 \leq\; B \;.\; \|x\|_{l_2}^2 \end{aligned} \quad (9)$$

With the help of Parseval's theorem it is easy to show that the energy conservation property is preserved

$$\|x\|_{l_2}^2 \;= \|c_{d_0}\|_{l_2}^2 \;+\; \sum_{i=1}^{d_0} \|d_i\|_{l_2}^2 \quad (10)$$

By definition, $c_i(k) = \langle x(l), h_i(l-k)\rangle$ and $d_i(k) = \langle x(l), g_i(l-k)\rangle$, where $\langle .,. \rangle$ is the corresponding inner product. The fundamental difference with an orthogonal system is that the representation may be redundant, this property together with the definition of wavelet coefficients in (3), leads to the simple reconstruction formula

$$x(l) \;=\; \sum_{k\,\in\,Z} c_{d_0}(k) h_{d_0}(l-k) + \sum_{i=1}^{d_0} \sum_{k\,\in\,Z} d_i(k) g_i(l-k) \quad (11)$$

3 Multiscale feature extraction

The feature extraction scheme consists of three main stages given in fig. 1. Basically the purpose of the filter is to extract local frequencies of the textures,

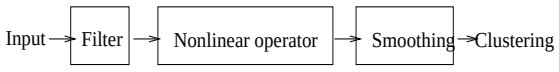

Figure 1: Fast iterative implementation of the algorithm used for extracting texture features

a subsequent nonlinear stage followed by a smoothing filter (both these constitute the local energy extimator). The objective of local energy estimator, is to estimate the energy of the filter ouput in a local region.

The wavelet function in 2 dimensions is defined by $\psi_a(\vec{b}) = \frac{1}{\sqrt{a}}\,\psi(\frac{\vec{x}-\vec{b}}{a})$. The directional information, can be incorporated in the wavelet function, by including a rotational parameter in it [13].

$$\psi_{a,\theta}(\vec{b}) = \frac{1}{a}\psi(R^\theta(\frac{\vec{x}-\vec{b}}{a})) \quad (12)$$

where R^θ is the rotation operator denoted by the matrix

$$\begin{pmatrix} \cos\theta & -\sin\theta \\ \sin\theta & \cos\theta \end{pmatrix}$$

Now if the wavelet is circularly symmetric $i.e$ R^θ has no influence in (12), such an wavelet would generate rotation invariant features. Therefore the wavelet function has to satisfy two conditions one is $\hat{\psi}(0) = 0$, which implies that the wavelet function has to be a zero mean function and $\hat{\psi}(\vec{r},\theta) = \hat{\psi}(\vec{r},0)$, this ensures that the rotation operator has no effect in (12).

We have chosen the wavelet used by Mallat in [14], which is the second derivative of a smoothing function. This choice have been made because this closely approximates the second derivative of Gaussian, which has circular symmetry and the basis functions are symmetrical, which means that there is no phase distortion.

3.1 Multiscale wavelet representation

The transform employed in this work is based on non-orthogonal (redundant) discrete wavelet frames introduced by Mallat [15] fig. 2. Let $\phi(x,y)$ be a smoothing function. We call the smoothing function the impulse response of a lowpass filter with a total mass of one and compact support, i.e.

$$\begin{aligned} &\textstyle\int_{-\infty}^{\infty}\int_{-\infty}^{\infty} \phi_s(x,y)dxdy = 1 \text{ and } \exists \epsilon > 0 : \phi_s(x,y) = 0, \\ &\forall \mid x \mid, \mid y \mid > \epsilon. \end{aligned} \quad (13)$$

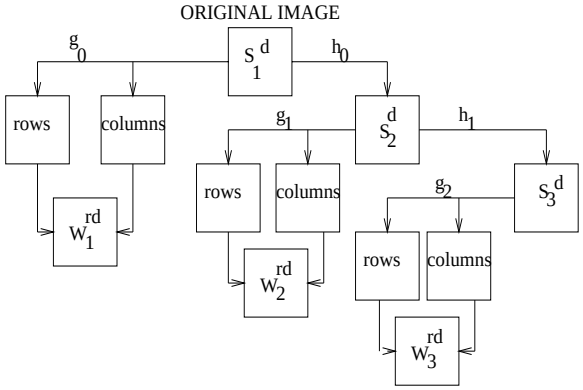

Figure 2: The wavelet decomposition scheme

Supposing $\phi(x,y)$ is differentiable, we define two wavelet functions, $\psi^1(x,y)$ and $\psi^2(x,y)$ such that,

$$\psi^1(x,y) = \frac{\partial^2\phi(x,y)}{\partial^2 x} \text{ and } \psi^2 = \frac{\partial^2\phi(x,y)}{\partial^2 y} \qquad (14)$$

Let,

$$\psi^1_s(x,y) = \frac{1}{s^3}\psi^1(\frac{x}{s},\frac{y}{s}) \text{ and } \psi^2_s(x,y) = \frac{1}{s^3}\psi^2(\frac{x}{s},\frac{y}{s}) \qquad (15)$$

be the dilations of the functions ψ^i by a factor s and $\phi_s(x,y) = \frac{1}{s}\phi(\frac{x}{s})$ the dilation of $\phi(x,y)$ by s.

Let $I(x,y)$ be an image in 2-D and $I(x,y) \in L^2(R)$. The wavelet transform of $I(x,y)$ at scale s has two components defined by,

$$w^1_s(x,y) = I * \psi^1_s(x,y) \text{ and } w^2_s(x,y) = I * \psi^2_s(x,y) \qquad (16)$$

s is the scale parameter which commonly is set equal to 2^i with $i = 1,\cdots,d_0$. This yields the traditional octave band wavelet transform of depth d_0. w^1_s and w^2_s are referred to as the detail images, since they contain the horizontal and vertical frequency informations of I at scale s.

This transform is computed by iterative filtering by a set of lowpass filters h_i associated with the smoothing function ϕ and bandpass filters g_i associated with the wavelets ψ^1 and ψ^2. These filters have finite impulse responses, which makes the transform fast and easy to implement.

$$\begin{aligned} c_{2^{i+1}}(x,y) &= [h_{i,x} * [h_{i,y} * c_{2^i}]](x,y) \\ w^1_{2^{i+1}}(x,y) &= [\delta_{i,x} * [g_{i,y} * c_{2^i}]](x,y) \\ w^2_{2^{i+1}}(x,y) &= [g_{i,x} * [\delta_{i,y} * c_{2^i}]](x,y) \end{aligned} \qquad (17)$$

$c_1 I$ is the original image and δ is the Dirac filter whose impulse response equals 1 at 0 and 0 otherwise. $*$ denotes the convolution operator. $A * (B * C)$ denotes separate convolution of the rows and columns respectively of the image A with 1-D filters B and C.

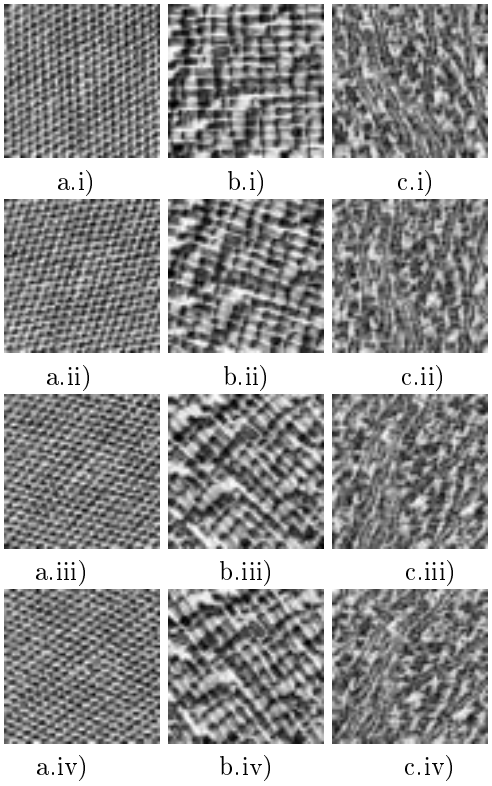

Figure 3: Rotated samples (0^0, 20^0, 45^0 and 55^0) of some of the textured images used in our experiment

Then the wavelet representation of depth d_0 of the image $I(x,y)$ consists of the low resolution images $\{c_{2^i}\}$ and detail images $\{w^j_{2^i}\}$ for $\{j = 1,2\}$ and $\{i = 1,\cdots,d_0\}$.

3.2 Texture features computation

Feature extraction is a crucial step in accomplishing reliable classification. A good feature representation should be consistent among the pixels with the same class, while as disparate as possible between classes for authentic and reliable classification. This means that it should reflect some global view while keeping some discrimination capability at the pixel level. Therefore the problem in general is one of spatial- spatial frequency analysis. We now discuss the computation of the rotation invariant parameters from wavelet transformed images.

Substitution of (14) and (16) in (15) yields the following,

$$\begin{aligned} \begin{pmatrix} w^1_s(x,y) \\ w^2_s(x,y) \end{pmatrix} &= s^2 \begin{pmatrix} \frac{\partial^2}{\partial^2 x}(I * \phi_s)(x,y) \\ \frac{\partial^2}{\partial^2 y}(I * \phi_s)(x,y) \end{pmatrix} \\ &= s^2\nabla^2(I * \phi_s)(x,y) \end{aligned} \qquad (18)$$

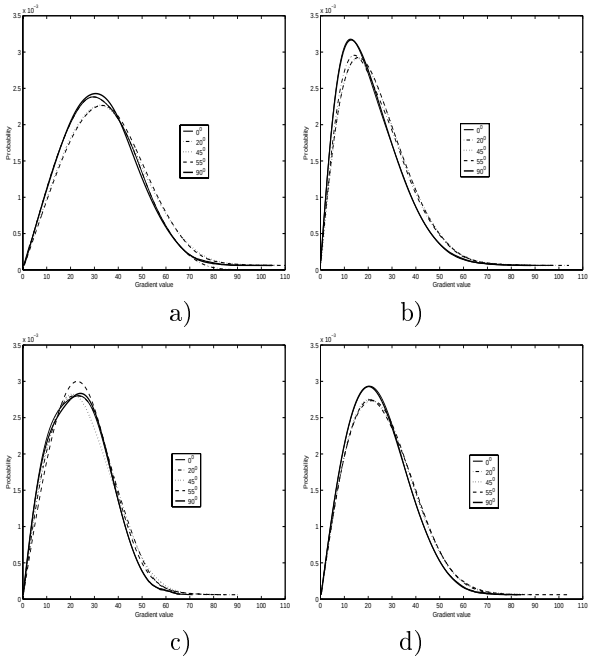

Figure 4: Gradient magnitude histogram plots of textures shown in figure 2 for textures a)2.a.i - 2.a.v b)2.b.i - 2.b.v c)2.c.i - 2.c.v d)2.d.i - 2.d.v

where ∇^2 denotes the Laplacian. It defines edge magnitudes of the image and since it has the same property in all directions is invariant to rotations in the image. That is the wavelet transform of an image consists of the components which give a measure of the edge magnitudes of the image, smoothed by the dilated smoothing function ϕ_s. The edge magnitudes of the image is given as,

$$w_s^r(x,y) = \sqrt{\left(w_s^1(x,y)\right)^2 + \left(w_s^2(x,y)\right)^2} \qquad (19)$$

The $w_s^r(x,y)$ contain a measure of the edge magnitude at (x,y), which is proportional to the magnitude of the local gray level variation of the image and clearly yields a rotation invariant multiscale representation $h_s = \{(w_s^r)_{(s=1,\cdots,2^{d_0})}, c_{2^{d_0}}\}$.

Figure 3 shows some of the textured images that we have used to generate the composite textures used in our experiment. We find out the histograms of the gradient values given by (19) of these textures at different rotations. The histograms so obtained has many local minima and maxima which can be removed by local smoothing of the histogram. This is accomplished by local averaging of neighboring histogram elements.

We have taken three adjacent elements at a time and the process is repeated for a number of iterations. A plot of these histograms after smoothing is given in fig. 3 to give a feeling that the edge magnitude of the textures are indeed rotation invariant. We calculate the first, second and the third order moments of the unrotated texture edge magnitude histogram and also its several rotated versions, to measure the similarity between these histograms, which is given in table 1.

Texture data	Rotation in deg.	Order of moments		
		First	Second	Third
Texture 1	unrotated	1.126	0.0014	0.0016
	20	1.127	0.0014	0.0016
	45	1.128	0.0014	0.0016
	55	1.129	0.0014	0.0016
	90	1.126	0.0014	0.0016
Texture 2	unrotated	1.288	0.0024	0.0029
	20	1.307	0.0023	0.0030
	45	1.313	0.0023	0.0031
	55	1.317	0.0024	0.0031
	90	1.291	0.0023	0.0029
Texture 3	unrotated	1.411	0.0029	0.0041
	20	1.444	0.0028	0.0039
	45	1.419	0.0029	0.0042
	55	1.432	0.0030	0.0043
	90	1.405	0.0029	0.0040
Texture 4	unrotated	1.334	0.0024	0.0032
	20	1.339	0.0024	0.0033
	45	1.336	0.0024	0.0032
	55	1.341	0.0024	0.0033
	90	1.331	0.0024	0.0032

Table 1. Moments of the magnitude histograms tabulated for comparing the similarity between the unrotated texture histograms and their rotated versions.

The moments so calculated suggest that the texture features are indeed rotation invariant.

3.3 Local energy estimation

The next step is to estimate the energy of the filter responses in a local region around each pixel. The local energy estimate is utilized for the purpose of identifying areas in each channel where the bandpass frequency components are strong resulting in a high energy value and the areas where it is weak into a low energy value. Energy is usually defined in terms of a squaring nonlinearity. However in a generalized energy function, other alternatives are used. We simply compute the average absolute deviation from the mean in small overlapping windows. One reason for choosing this nonlinear operator is that it is parameter free, meaning it is independent of the dynamic range of the input image and also of the filter amplification.

The local energy $e_s(i,j)$ around the i,j^{th} pixel is

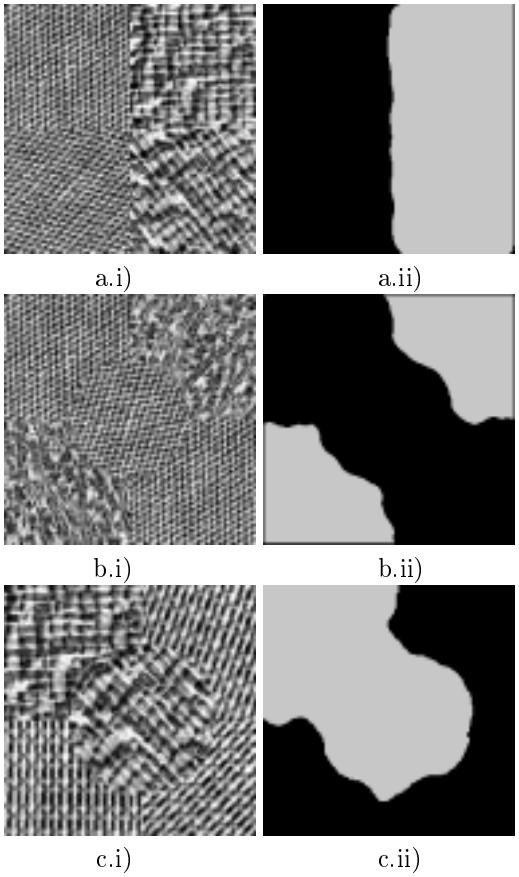

Figure 5: a.i-c.i) Composite textured images with their corresponding segmented outputs (K=2)

formally given as,

$$e_s(i,j) = \frac{1}{R} \sum_{m=1}^{W} \sum_{n=1}^{W} \mid (h_s(m,n) - \overline{h}_s(i,j)) \mid \quad (20)$$

where, W is the window size and $R = WXW$, while $\overline{h}_s(i,j)$ is the mean around the $(i,j)^{th}$ pixel and $h_s(i,j)$ is the filtered image at different scales for $s = 1, \cdots, 2^{d_0}$.

The nonlinear transform is succeeded by a Gaussian low pass (smoothing) filter of the form,

$$H_G(u,v) = \frac{1}{2\pi\sqrt{\sigma}} e^{\frac{1}{2\sigma^2}(u^2+v^2)} \quad (21)$$

Formally, the feature image $f_s(i,j)$ corresponding to filtered image $h_s(i,j)$ is given by,

$$f_s(i,j) = \frac{1}{G^2} \sum_{(a,b) \in G_{ij}} \mid \Psi(h_s(a,b)) \mid \quad (22)$$

where $\Psi(\cdot)$ is the local energy estimator and G_{ij} is a GXG window centered at pixel with coordinates (i,j). The size G of the smoothing or the averaging window in equation (22) is an important parameter. More reliable measurement of texture feature calls for larger window sizes. On the other hand, more accurate localization of region boundaries calls for smaller windows. This is because averaging blurs the boundaries between textured regions. Another important aspect is that, Gaussian weighted windows are naturally preferable over unweighted windows, because, the former are likely to result in more accurate localization of texture boundaries.

The images resulting from these operations are the feature maps $F_s(i,j)$ at different scales.

3.4 Unsupervised classifier

Having obtained the feature images, the main task is to integrate these feature images to produce a segmentation. We define a scale - space signature as the vector of features at different scales taken at a single pixel in an image,

$$\overline{F}(i,j) = [F_0(i,j), F_1(i,j), F_2(i,j), \ldots, F_N(i,j)] \quad (23)$$

Suppose these scale-space signatures are considered as feature vectors in a feature space. If the signatures of one texture are distinct from the signatures of another texture a pattern recognition system can be used to identify several different textured regions in the scale space.

Let us assume that there are M texture categories. $C_1, \ldots, C_M$, present in the image. If our texture features are capable of discriminating these categories then the patterns belonging to each category will form a cluster in the feature space which is compact and isolated from clusters corresponding to other texture categories. Pattern clustering algorithms are ideal modes for forming such clusters in the feature space. Segmentation algorithm accept as input a set of features and put a consistent labeling for each pixel. Fundamentally this can be considered a multidimensional data clustering problem. Clustering algorithms that have been previously used for texture segmentation can be divided into two categories : supervised and unsupervised segmentation.

We emphasize on the feature extraction (representation) part in this work. So we have used a traditional K-means clustering algorithm. Although other sophisticated algorithms like watershed clustering could have been used. We normalize each scale-space signature by dividing each value in the signature by the signature's total magnitude. This is to ensure that no particular feature dominates the feature space. For the image I

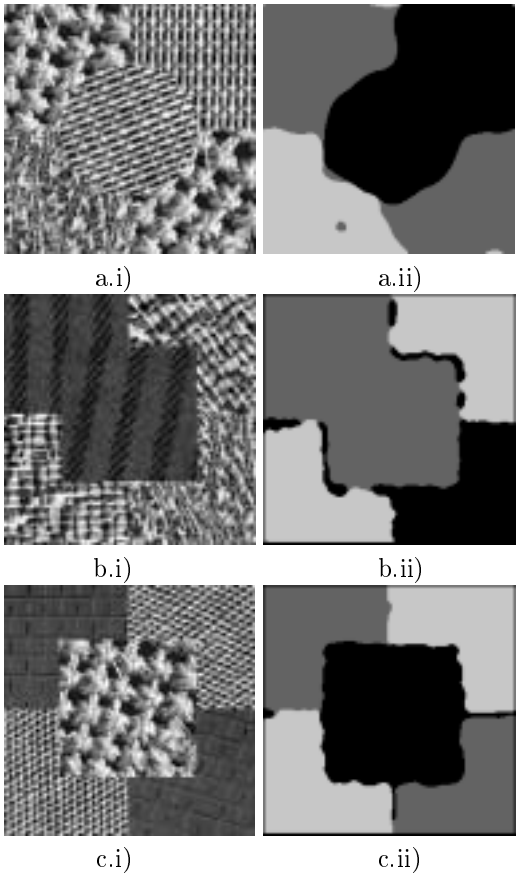

Figure 6: Composite textured images with their corresponding segmented outputs (K=3)

the normalized scale-space signature is,

$$\overline{F}(i,j) = \left[\frac{F_0(i,j)}{\sum_{k=0}^{N} F_k(i,j)}, \ldots, \frac{F_N(i,j)}{\sum_{k=0}^{N} F_k(i,j)} \right]$$

4 Experimental results

We have experimented our segmentation algorithm on a number of textured images taken from the Brodazt album which clearly exhibit anisotropy. We have considered both integer and fractional rotations, because integer rotations are distortion free and it is very difficult to characterize fractionally rotated textures. Several rotations have been considered, like 15.5^0, 20^0, 37.5^0, 45^0, 55^0, 60^0 and 90^0. Several composite textured images have been generated from the rotated versions of these textured images. Since we are mainly interested in the effectiveness, reliability and robustness of the rotation - invariant features that are extracted rather than the segmentation performances, we have experimented on composite textured images consisting of a moderate number of texture classes.

Figure 5 show two class test images that we have worked on, which consist of 5 regions, out of which two regions are unrotated textures and the rest three comprise of rotated textures. The images were decomposed into three levels of resolution as given in fig. 2. We have taken into account all the three detail images and two of the low frequency images leaving out the lowest frequency image at the third level of resolution, to estimate the local energies around each pixel at different scales. That is in all we are left with only five feature elements which means a huge reduction in the dimensionality of the feature space, compared to other methods so far reported in the literature. Segmentation was performed with K-means clustering with fixed K=2, results are shown in figure 5. Percentage of correct classification have been taken as the measure of performance in this work. The classification percentage for figures 5a.i, 5b.i and 5c.i are 99.31 %, 98.93 % and 97.41 % respectively.

Figure 6 show some composite textured images that we have tested on, which comprise of three different texture classes. The images consist of 5 regions with three unrotated textured regions and two rotated textured regions. Segmentation is carried out using K-means clustering with fixed K=3, the experimental results are shown in fig 6. The classification percentages for test images 6a.i, 6b.i and 6c.i are 98.24 %, 97.61 % and 98.49 % respectively.

5 Conclusion

This paper studies the issue of rotation-invariance for texture segmentation. Simple and computationally efficient features have been extracted based on the fact that circularly symmetric wavelets give rotationally - invariant features, as these wavelets are independent of orientation. We have seen that wavelet frame analysis is appropriate over the standard subsampled wavelet analysis for rotational invariance. We have also seen that the features that we have extracted are really invariant to rotation by studying the gradient magnitude histograms of the several rotated versions of the same texture class. Another important aspect of our algorithm is that we make use of only five features to achieve the desired segmentation and this entails a huge reduction in feature dimensionality.

Studying the results of our experiment over several composite textured images we can conclude that our scheme performs appreciably well. But some edge inaccuracies are observed apart from some misclassification. One reason for this might be because for the purpose of segmentation the features that are computed are pixel based, i.e. features are the measure of local energies over a small window around each pixel.

A proper choice of this window size is very essential. The window size should be such that it captures the total periodicity of the microtextures of each class this calls for larger window size, where as for accurate texture boundary localization between classes the window size should be small.

It is to be noted that we have not done any post-processing over the classified images. Where postprocessing like median filtering or simple morphological operation like dilation would have definitely improved the classification results. But inspite of that we have achieved good classification and hence we can claim that our approach gives an effective rotation invariant texture segmentation.

Another important point to be noted is that, the standard two-band wavelet decomposition imply fine frequency resolution in the lower frequency band than in the higher band and hence are not suitable for the analysis of high frequency signals with relatively narrow bandwidth. Therefore we conjecture that an M-band wavelet analysis where M is greater than two can characterize textures better than the two-band wavelets. Since our segmentation algorithm is based on the concept that two different texture classes comprise of different signal energies. So the accuracy of our algorithm lies on the fact that how effectively we can characterize each texture in terms of its signal energies. This in turn demands for decomposition of each textures into a large number of subbands. So we are of the opinion that M-band wavelets are more suitable for this purpose of segmentation. We have already done a work in support of this [16].

References

[1] M. Tuceryan and A. K. Jain, "Texture analysis," in *Handbook of Pattern Recognition and Computer vision*, pp. 235–276, World Scientific, 1993.

[2] T. Chang and C. C. J. Kuo, "Texture analysis and classification with tree structured wavelet transform," *IEEE Transactions on Image Processing*, vol. 2, no. 4, pp. 42–44, 1993.

[3] J. L. Chen and A. Kundu, "Rotation and gray scale transform invariant texture identification using wavelet decomposition and hidden markov model," *IEEE Trans. Patt. Anal. Mach. Intell.*, vol. 16, no. 2, pp. 208–214, 1994.

[4] S. Mallat, "A theory for multiresolution signal decomposition: The wavelet representation," *IEEE Trans. Patt. Anal. Mach. Intell.*, vol. 11, no. 7, pp. 674–693, 1989.

[5] A. Laine and J. Fan, "Texture classification by wavelet packet signatures," *IEEE Trans. Patt. Anal. Mach. Intell.*, vol. 15, no. 11, pp. 1186–1190, 1993.

[6] M. Unser, "Texture classification and segmentation using wavelet frames," *IEEE Transactions on Image Processing*, vol. 4, no. 11, pp. 1549–1560, 1995.

[7] R. L. Kashyap and A. Khotanzed, "A model-based method for rotation invariant texture classification," *IEEE Trans. Pattern Anal. Machine Intell. PAMI*, vol. 8, no. 4, pp. 472–481, 1986.

[8] F. S. Cohen, Z. Fan, and M. A. Patel, "Classification of rotation and scaled textured images using gaussian markov random field models," *IEEE Trans. Pattern Anal. Machine Intell. PAMI*, vol. 13, no. 2, pp. 192–202, 1991.

[9] W. R. Wu and S. C. Wei, "Rotation and gray scale transform invariant texture classification using spiral resampling, subband decomposition and hidden markov model," *IEEE Trans. on Image Process.*, vol. 5, no. 10, pp. 1423–1434, 1996.

[10] S. R. Fountain and T. N. Tan, "Efficient rotation invariant texture features for content - based image retrieval," *Pattern Recognition*, vol. 31, no. 11, pp. 1725–1732, 1999.

[11] M. Acharyya and M. K. Kundu, "Robust texture classification using wavelet frames," *Accepted in Image Processing and Communication*, 2000.

[12] G. Strang and T. Nguyen, *Wavelets and Filter Banks*. Wellessley - Cambridge Press, 1996.

[13] I. Daubechies, *Ten Lectures on Wavelets*. Philadelphia: Soc. Ind. Applied Math, 1992.

[14] S. Mallat, "Zero-crossings of a wavelet transform," *IEEE Trans. Patt. Anal. Mach. Intell.*, vol. 37, no. 4, pp. 1019–1033, 1993.

[15] S. Mallat and S. Zhong, "Characterization of signals from multiscale edges," *IEEE Trans. Patt. Anal. Mach. Intell.*, vol. 14, no. 7, pp. 710–732, 1992.

[16] M. Acharyya and M. K. Kundu, "An adaptive approach to unsupervised texture segmentation using m-band wavelet," *Communicated*, 1999.